Bioorganic Chemistry **30,** 163–187 (2002)
doi:10.1006/bioo.2002.1255

Large-Scale Motions within Ribosomal 50S Subunits as Demonstrated Using Photolabile Oligonucleotides

Hyuk-Soo Seo and Barry S. Cooperman[1]

Department of Chemistry, University of Pennsylvania, Philadelphia, Pennsylvania 19104

Received February 5, 2002

Photolabile oligonucleotides (PHONTs) bind to rRNA sequences to which they are complementary and, on photolysis, incorporate into neighboring ribosomal components. Here we report on photocrosslinking results obtained with PHONTs targeting 23S rRNA nucleotides 1882–1892, in the long lateral arm of the 50S subunit (PHONT 1892), and 1085–1093, in the L11 binding domain (PHONT 1093). Photolysis of the PHONT 1892.50S and PHONT 1093.50S complexes leads to formation of 'long-range' crosslinks from C1892 to U1094/A1095 and G1950, and from G1093 to U1712/1716 and U1926, that are clearly incompatible with published crystal structures of 50S subunits. These results provide strong evidence that within the 50S subunit (a) the L11 binding domain can extend in an arm-like fashion, accessing large areas of the ribosome, and (b) the lateral arm can bend about the noncanonical helix at its center. Such motions may have functional relevance in identifying regions that undergo major conformational change as the ribosome moves through its catalytic cycle.

Key Words: 50S structure; PHONT; conformational lability; L11 binding domain; lateral arm.

INTRODUCTION

In 1962, prior to the determination of protein structures by crystallography and NMR, Singh, Thornton, and Westheimer introduced the use of a photolabile derivative of the active site serine of chymotrypsin to determine, via photoinduced crosslinking, the identity of proximal side chains at the enzyme active site (*1*). Since this seminal article, photoinduced crosslinking and the related approach of photoaffinity labeling have been used extensively to explore binding sites of a large number of biological macromolecules (*2*), particularly those deemed too large for direct structure elucidation. In recent years we have used photoinduced crosslinking to examine ribosome structure (3–6). In our studies radioactive, photolabile derivatives of oligonucleotides (PHONTs),[2] having sequences complementary to rRNA sequences, are bound to their

[1] To whom correspondence and reprint requests should be addressed. Fax: (215) 898-2037. E-mail: cooprman@pobox.upenn.edu.

[2] Abbreviations used: EF-G, elongation factor G; PAGE, polyacrylamide gel electrophoresis; PHONT, photolabile oligonucleotide; RP-HPLC, reverse phase high performance liquid chromatography; RT, reverse transcriptase; TS, thiostrepton; XLR, long-range cross link.

0045-2068/02 $35.00

targeted sequences in intact ribosomes or ribosomal subunits, and, on photolysis, incorporate into ribosomal components that can subsequently be identified. This work initially had as a goal the generation of constraints that, in concert with other kinds of information (footprinting and other chemical modification approaches, immunoelectron microscopy, image reconstruction of electron micrographs), could be used to construct three-dimensional models of ribosome structure (*6–9*). This goal has largely been rendered obsolete by the publication in the last 2 years of high resolution X-ray structures of 30S and 50S subunits of bacterial ribosomes, and somewhat lower resolution structures of 70S ribosomes, which provide an exquisitely detailed picture of how various elements (proteins, RNA helices) fit together in forming this fascinating and important macromolecular structure (*10–15*).

Now that the basic structure of the ribosome is known, attention in the field is focusing on the nature of conformational changes that occur as the ribosome exerts its complex catalytic function, involving the movement of mRNA and tRNAs across its surface, in a highly choreographed sequence of events requiring catalysis by a host of protein factors. Image reconstruction of electron micrographs of ribosomes from *Escherichia coli* show clear evidence for large-scale conformational changes between ribosomes flash-frozen in different functional forms (*16–18*), and similar evidence has been obtained for eucaryotic ribosomes (*19*), although the limited resolution of such experiments does not permit precise identification of the ribosomal components involved.

Against this background, photocrosslinking studies remain important because of their potential for providing information about ribosome conformations that may otherwise be difficult to obtain. As they are performed in solution, they access conformations that may be different from those seen in crystals. Also, as the probability of a photocrosslink being formed depends on several factors (proximity, orientation, chemical selectivity) they can reveal the presence of conformations present in relatively small amounts, which might be missed by image reconstruction procedures. Furthermore, intrinsic to such studies is the identification of specific sites within the ribosome that may be involved in large scale motions.

The PHONT approach is particularly suitable, because it allows facile targeting of rRNA sequences of particular interest. Detailed comparison of the crystal structures of 50S subunits from *Thermus thermophilus* (*12*), *Haloarcula marismortui* (*11*), and *Deinococcus radiodurans* (*15*) have, in the context of substantial overall similarity, identified several 23S rRNA regions that are either known or thought to be conformationally labile in isolated 50S subunits. These areas are prime candidates for where functionally relevant conformational changes might occur. Here we report on photocrosslinking results obtained with PHONTs (Fig. 1A) targeting two of these regions. PHONT 1892 is complementary to nucleotides 1882–1892, a sequence in helix 68 that falls between two functionally important regions, helix 69, which is important for tRNA binding (*20*), and helix 66, which forms part of the binding site for L2 (*21*), a protein that appears to play an important allosteric role in controlling peptidyl transferase activity (*12,22–24*). PHONT 1093 is complementary to nucleotides 1085–1093, falling in a region (helix 44) that has been implicated in both elongation factor G (EF-G) and thiostrepton (TS) binding (*25–28*).

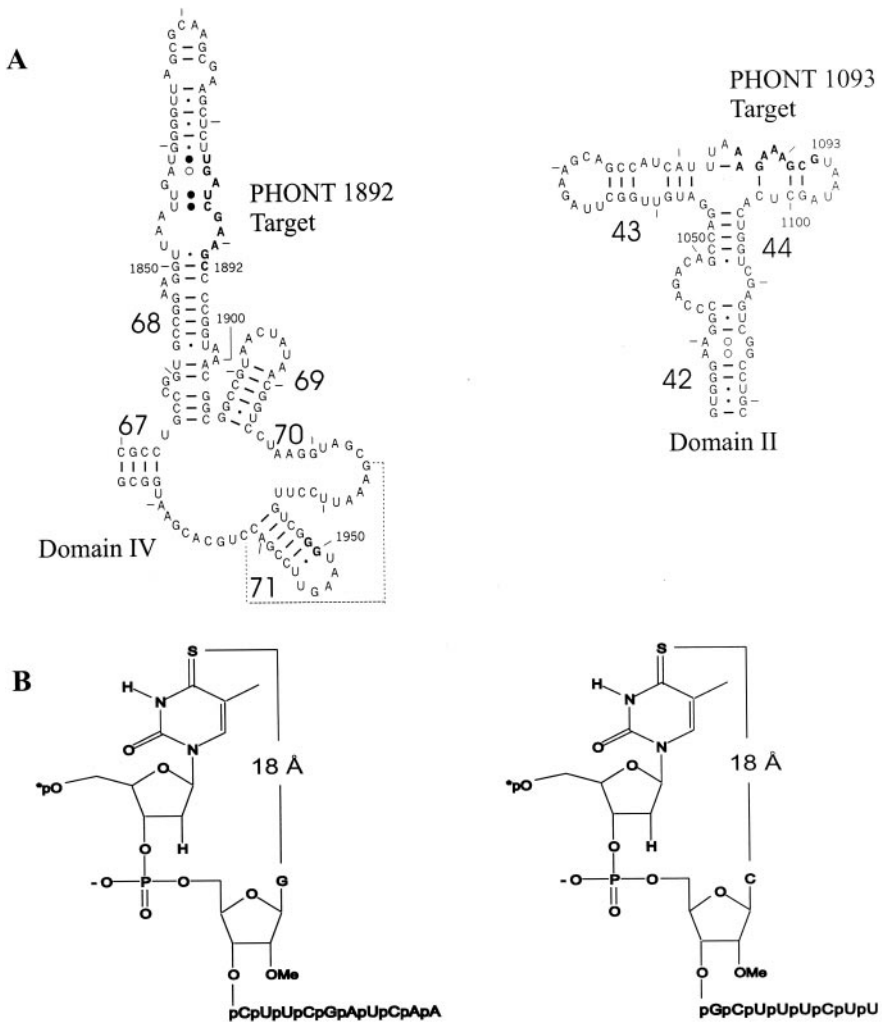

TARGET 1 : 23S rRNA 1882-1892 3'- CGAAGCUAGUU-5'

PHONT 1892: 5'-s^{4}dT-2'-O-methyloligoRNA-GCUUCGAUCAA-3'

CHASE 1892: 5'-dT-2'-O-methyloligoRNA-GCUUCGAUCAA-3'

MISMATCH 1892: 5'-2'-O-methyloligoRNA-GCU**AGC**AUCAA-3'

TARGET 2 : 23S rRNA 1085-1093 3'- GCGAAAGAA-5'

PHONT 1093 5'-s^{4}dT-2'-O-methyloligoRNA-CGCUUUCUU-3'

CHASE 1093 : 5'-dT-2'-O-methyloligoRNA-CGCUUUCUU-3'

MISMATCH 1093: 5'-2'-O-methyloligoRNA-C**CG**UUUCUU-3'

FORMATCH 1093-1 (227-218) 5'-2'-O-methyloligoRNA-**U**G**A**UUUCUU-3

FORMATCH 1093-2 (1814-1805) 5'-2'-O-methyloligoRNA-C**A**CUUUC**G**U-3'

FORMATCH 1093-3 (1936-1927) 5'-2'-O-methyloligoRNA-CGCU**AC**CUU-3'

FIG. 1. (A) Targeted sites (in bold) within 23S rRNA for PHONTs 1892 and 1093. (B) The structures of PHONT 1892 and PHONT 1093 and the sequences of PHONT, CHASE, MISMATCH, and FORMATCH oligonucleotides. Nonmatching nucleotides are in bold and underlined.

MATERIALS AND METHODS

Except as specified below, materials were obtained and methods were performed as described elsewhere (*3,4*).

Materials

Oligonucleotides. Oligonucleotides used in photocrosslinking experiments are presented in Fig. 1B, and chimeric oligonucleotides used to generate precise cleavage sites for RNase H are presented in Table 2. Each was prepared using phosphoramidite chemistry, and purified using HPLC (Nucleic Acid Facility, University of Pennsylvania). ^{32}P-labeled oligonucleotides, whether used in binding (p*CHASE 1892 and p*CHASE 1093), photoincorporation (p*PHONT 1892 and p*PHONT 1093), or reverse transcription experiments were prepared using T4 polynucleotide kinase (New England Biolabs) and [γ-^{32} P]ATP. p*PHONT 1892, p*PHONT 1093, p*CHASE 1892, and p*CHASE 1093 were shown to be radiochemically homogeneous by autoradiography of a urea–PAGE (20% acrylamide in TBE buffer) analysis. Fortuitous matches to targeted sequences, FORMATCHs, were detected with the program AMPLIFY (authored by Bill Engels; www.wisc.edu/genestest/CATG/amplify).

E. coli (Q13 strain) 50S subunits were prepared as described (29). 50S subunit pellets were suspended in TKM_{10} buffer (A_{260}, 20–30), flash-frozen, and stored at −70°C. Prior to use in binding or photoincorporation experiments, subunits were activated by incubation at 37°C for 20 min in TKM_{10} buffer. Thiostrepton was from Sigma.

Buffers. TKM_{10} buffer: 50 mM Tris–HCl (pH 7.6), 50 mM KCl, and 10 mM $MgCl_2$; Binding buffer: 40 mM Tris–HCl (pH 7.6), 60 mM KCl and 10 mM $MgCl_2$; Reverse transcriptase buffer: 50 mM Tris–HCl (pH 8.3), 50 mM KCl, 10 mM $MgCl_2$, 10 mM DTT, and 0.5 mM spermidine. TBE buffer: 89 mM Tris base, 89 mM boric acid, 2 mM EDTA, pH 8.3. $T_{25}N_{125}D_{1.25}$ buffer: 25 mM Tris–HCl (pH 7.6), 125 mM NaCl, and 1.25 mM DTT.

Methods

Photolysis. In the standard photolysis experiment, 150 pmol of 50S subunit was incubated with 50 pmol of p*PHONT and in the absence or presence of excess CHASE, MISMATCH or FORMATCH oligonucleotides in 100 μl of binding buffer. After 5 min incubation at 37°C followed by 30–60 min on ice, samples were irradiated for 5 min in a Rayonet RPR Photochemical Reactor equipped with RPR-3500 Å UV-lamps (310–370 nm, max at 350 nm—Southern New England Ultraviolet Co., Branford, CT). 2-Mercaptoethanol was added immediately after photolysis (final concentration, 20 mM) and 50S subunits were precipitated in 2 volumes of 10% 2-mercaptoethanol in ethanol (v/v) at −20°C for at least 2 h.

RNA extraction from 50S subunits. 50S pellets were washed once with 70% ethanol, dissolved in RNA extraction buffer (0.3 M NaOAc, 3 mM EDTA, and 0.5% SDS) and extracted twice with phenol, once with phenol:chloroform:isoamyl alcohol (25:24:1) and finally once with chloroform. Extracted rRNA was then precipitated with 2.5 vol of cold EtOH (90 min, −20°C). Precipitated rRNA was washed once

with cold 70% EtOH, and finally dissolved in appropriate volume, typically 20–30 μl, of 1 mM EDTA.

RNase H analyses. In a typical analysis, 10 pmol of extracted rRNA was hybridized with 20 pmol of one or two oligoribonucleotides (cDNA or chimeric oligonucleotide—Table 2) by heating at 55°C for 5 min and annealing for 15 min at 32°C in $T_{25}N_{125}D_{1.25}$ buffer. Mg^{2+} concentration was adjusted to 10 mM and the RNA was digested with 2 units of RNase H (Promega) for 30 min at 32°C. Following digestion, samples were heated in 70% formamide/bromphenol blue/xylene cyanol sample buffer and separated by urea-PAGE (5–10% acrylamide in TBE). Determination of relative yields of RNase H fragment labeling required: (a) either quantitative scanning of the autoradiogram or direct measurement of the ^{32}P content of labeled gel slices (both methods gave equivalent results), and (b) estimation of the yield of fragment formation (i.e., cleavage efficiency) in the presence of the two added complementary oligonucleotides that generate the RNase H cleavage sites. Such estimates were obtained by hybridizing 50S rRNA with the nucleotides in question, and, following RNase H digestion, urea–PAGE separation of products, and methylene blue staining of the gel, quantifying the intensity of the stained band (MICROTEK, ScanMaker 9600 XL) corresponding to the expected fragment, using the intensity of the 5S rRNA band as an internal standard, and assuming that band intensity/mole is proportional to fragment length. Gels were sandwiched between two sheets of cellophane and dried thoroughly prior to scanning.

Reverse transcriptase analyses. Preparation of PHONT-labeled 50S RNA annealed with ^{32}P-labeled oligo cDNA promer was carried out as described (*3*), except the first heating step was carried out at 65°C rather than 70°C, and better results were obtained with reverse transcriptase from Sekkagaku in place of that from Promega. Extracted RNase H fragments (see below) were analyzed similarly, except that the rRNA was labeled with p*PHONT.

RNase H fragment extraction. RNase H fragments, resolved by urea–PAGE as described above, were eluted from the appropriate gel slice, typically $12 \times 2 \times 0.4$ mm, with 400 μl of eluting buffer (0.3M NaOAc, 1 mM EDTA and 2% SDS) by incubation at 42°C for 6 h. The resulting solution was extracted twice with phenol:chloroform:isoamyl,alcohol (25:24:1) and precipitated in 2.5 vol of cold EtOH, using glycogen (*30*) (Boehringer-Mannheim, 14 μg/ml) as carrier. The resulting pellet was dissolved in 1 mM EDTA.

RNase T1 digestion. In a typical digestion, extracted RNase H fragment, $\leq$0.4 μM, was incubated at 55°C for 5 min $\pm$ added cDNA (40 μM) in a final volume of 10 μl of RNAse T1 buffer (40 mM Tris–HCl (pH 7.6), 200 mM NaCl, 5 mM EDTA, and 1 mM DTT). After the sample was slow cooled to room temperature and incubated for 30 min on ice, 5 units of RNase T1 (5 units, Boehringer-Mannheim) were added and digestion was carried out for 12 h on ice. An additional 5 units of RNase T1 were then added, and incubation was continued for 2 h at 30°C. Loading dye was added to each tube and the samples were analyzed by 20% urea–PAGE.

Chemical footprinting. Chemical footprinting was performed as described (*3*) except 2 μl of DMS (1:30 dilution in ethanol) or 2 μl of kethoxal (37 mg/ml kethoxal in 20% ethanol) were used per 50 pmol 50S subunit in a total volume of 50 μl.

RESULTS

Noncovalent binding CHASE 1892 and CHASE 1093 to the 50S subunit. The 2′-O-methyloligoRNAs p*CHASE 1892 and p*CHASE 1093 (Fig. 1B) bind noncovalently to the 50S subunits with similar stoichiometries of ~0.3/50S subunit and with apparent K_d values of 5.0 ± 1.5 and 2.0 ± 0.2 μM, respectively (Fig. 2). These values fall within the range of values for K_d (0.02–31 μM) and stoichiometry (as high as 1.25, with most 0.1–0.7) found for oligonucleotide binding to ribosomal subunits by ourselves and others (*4,6,31–34*). Thiostrepton (TS), which binds to *E. coli* 50S subunits with a dissociation constant ≤0.01 μM (*35–37*), and appears to interact strongly with A1067 and more weakly with A1095 (*26*), inhibits p*CHASE 1093 binding in a noncompetitive manner (Fig. 1). The results obtained indicate that TS binding to the 50S subunit weakens p*CHASE 1093 binding by ~9-fold.

Site-specific photoincorporation of PHONTs. Photolysis of non-covalent complexes of 50S subunits with either p*PHONT 1892 or p*PHONT 1093 was generally performed at excess of 50S over PHONT in order to maximize photoincorporation from each high affinity site, as demonstrated above. No target site-specific labeling was seen for 5S rRNA. Evidence for target site-specific crosslinking into 23S rRNA was provided by the results displayed in Table 1, showing a large decrease in photoincorporation in the presence of the corresponding CHASE oligonucleotide, which should bind competitively to the target site. This contrasts with the lack of effect of added MISMATCH or FORMATCH oligonucleotides of similar length (Fig. 1B). As the name implies, MISMATCH oligonucleotides contain mismatched residues that weaken binding to the target site. FORMATCH oligonucleotides are complementary to nucleotide sequences within 23S rRNA or 5S rRNA that fortuitously match the

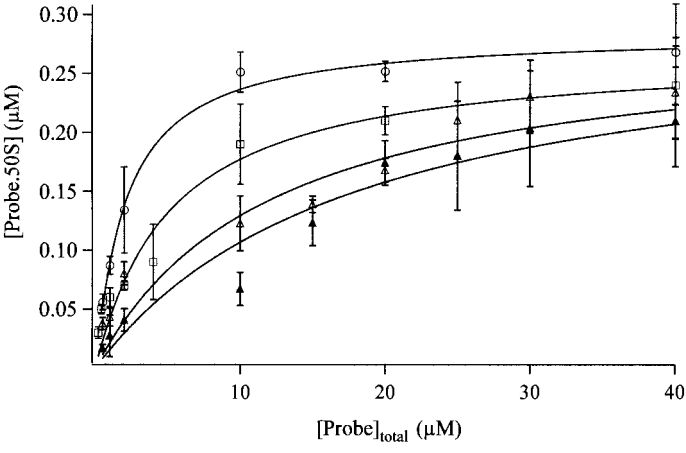

FIG. 2. Noncovalent binding to 50S subunits. 15 pmoles of 50S subunits were combined with varying amounts of ^{32}P-labeled CHASE oligonucleotides in binding buffer (total volume,15 μl), incubated at 37°C for 5 min and on ice for 2 h and filtered through Millipore 0.45 μm nitrocellulose filters. Measurements were performed in triplicate. Curves are simple binding isotherms fitted with the following $K_{d,app}$ values (μM): (□), p*CHASE 1892–1882, 5.0 ± 1.5; (○) , p*CHASE 1093 2.0 ± 0.2; (△), p*CHASE 1093 + 15 pmol of TS, 11.5 ± 0.9; (▲) p*CHASE 1093 + 150 pmol TS, 18 ± 2.

TABLE 1

Relative Photocrosslinking Yields[a]

	Standard	−UV[b]	CH[c]	MM[d]	FM[e]
p*PHONT 1892	1.0 (1.3 ± 0.2%)[f] (19 ± 3%)[g]	<0.009	0.07 ± 0.03	0.99 ± 0.08	—
p*PHONT 1093	1.0 (0.67 ± 0.03%)[f] (6.2 ± 0.3%)[g]	<0.009	0.23 ± 0.10	1.21 ± 0.27	0.99 ± 0.13

[a] After photolysis and separation by urea—PAGE (3.5% polyacrylamide), bands corresponding to [^{32}P]-labeled 23S rRNA are excised, mixed, with scintillation fluid (Ecolite, ICN), and radioactivity is measured. Unless otherwise indicated, relative values are given, with the value for the standard experiment (1.5 μM 50S subunits, 0.5 μM p*PHONT in binding buffer, 5-min irradiation, 37°C) set equal to 1.0.

[b] Not exposed to UV light.

[c] In the presence of added corresponding CHASE oligonucleotide (9 μM).

[d] In the presence of added corresponding MISMATCH oligonucleotide (9 μM).

[e] In the presence of added FORMATCH oligonucleotides (9 μM in each).

[f] The absolute level of crosslinking as percentage of p*PHONT that is eluted with 23S rRNA

[g] The absolute level of crosslinking as percentage of p*PHONT noncovalently bound to 50S subunits (Fig. 2) that is eluted with 23S rRNA

target sequence with no more than two mismatches. No such sequences were found for PHONT 1892, but three were found for PHONT 1093 (Fig. 1B). The lack of effect of all three of these FORMATCHs on PHONT 1093 photoincorporation provides clear evidence that such photoincorporation is coming from the target site, rather than from fortuitous sites.

Although both reverse phase HPLC and SDS–PAGE analysis showed photoincorporation into 50S proteins, neither analysis provided unambiguous evidence for target site-specific labeling (data not shown), and this labeling was not further pursued.

Partial localization of specifically labeled regions in 23S rRNA. Using the now standard approach (*3*), partial localizations of the photoincorporation sites of p*PHONTs 1892 and 1093 were achieved by RNase H cleavage of labeled 23S rRNA hybridized with a series of cDNA or chimeric oligonucleotides (Table 2) that, used together, generated fragments ~25–300 nt long over the whole 23S rRNA sequence. Fragments excised by RNase H were analyzed by denaturing urea-PAGE and autoradiography. When cDNA oligonucleotides are used, the apparent sizes of labeled fragments, as determined by comparison with RNA/DNA size markers, are typically 10–20 nts larger than would be expected for calculated unlabeled fragments, due to both the size of photoincorporated probe itself (10 or 12) and the multiple sites of RNase H hydolysis within a given cDNA-RNA heteroduplex. Use of chimeric oligonucleotides affords more precise fragment length, since RNase H cleavage is confined to one or two positions (Table 2).

A scan of the entire length of 23S rRNA showed that p*PHONT 1892 target site-specifically labels three 23S rRNA fragments, 1051–1274, 1680–1857, and 1857–2020 (Fig. 3A). Finer localization to fragments 1080–1111, 1845–1868, and 1910–1975 (Fig. 3B) was achieved using chimeric oligonucleotides (Table 2). As above,

TABLE 2

Chimeric Oligonucleotides Used for RNase H cleavage of 23S rRNA

Oligonucleotides	Expected cleavage sites with RNase H[a]	Sequence[b]
1051–1042	1050–1051	CTGTCUGGGC
1060–1051	1059–1060	ACATCCUGGC
1080–1071	1079–1080	TGATGGCUGC
1111–1102	1110–1111	TCGACCAGUG
1274–1265	1273–1274	TATCGUUACU
1700–1691	1699–1700	TCTCCCGAAG
1701–1688	1700–1701	TTCTCCCGAAGUUA
1742–1733	1741–1742	AGCTCCAUCC
1764–1751	1763–1764	GCTGGUAUCUUCGA
1816–1803	1815–1816	GTCCACUUUCGUGU
1845–1836	1844–1845	GCCGUGGCCC
1868–1859	1867–1868	GCTAACCCCA
1872–1859	1871–1872	TTGCGCUAACCCCA
1910–1897	1909–1910	CGGCCGCCGUUUAC
1975–1962	1974–1975	CGCCAUUCGUGCAG
2011–1998	2010–2011	ACTGAGUCUCGGGU

[a] Ref. (*44*).
[b] Deoxyribonucleotides (normal face) or 2′-OMe-ribonucleotides (underlined).

site-specificity is demonstrated by the effects of added CHASE 1892 and MISMATCH 1892. Similarly, target site-specific labeling by p*PHONT 1093 was first localized to fragments 1051–1274, 1700–1845, and 1845–2020, and subsequently to fragments 1051–1111, 1700–1742 and 1910–1975 (Fig. 3C–3E). The relative labeling yields of target site-specifically labeled RNase H fragments, corrected for RNase H cleavage efficiency, are presented in Table 3.

Thiostrepton effects on the photoincorporation of PHONTs 1892 and 1093. The effects of added TS on photoincorporation of p*PHONTs 1892 and 1093 are consistent with its tight binding to the H43/H44 region (Fig. 1A) of 23S rRNA. Thus, added at

FIG. 3. RNase H digestion analyses of p*PHONT-labeled 23S rRNA. Photolyses were carried out under standard conditions ([50S] = 1.5 μM, [p*PHONT] = 0.5 μM) (A–B): p*PHONT 1892. (-) lanes, no further addition during photolysis; (CH) or (MM) lanes, photolyses carried out in the presence of a 15-μM CHASE 1892 or MISMATCH 1892, respectively. (C–E): p*PHONT 1093. (-) lanes, no further addition during photolysis; (CH) or (M/F) lanes, photolyses carried out in the presence of a 15 μM CHASE 1093 or of a mixture of 15 μM each of MISMATCH 1093 and all three FORMATCH 1093s, respectively. Oligonucleotides used to generate RNase H sites are either cDNAs (complementary to sequences 1051–1042, 1274–1265, 1680–1671, 1857–1848, and 2020–2011) or chimeric oligonucleotides, as listed in Table 2. Lanes are labeled using the highest base number for each sequence. For example, 1051–1274 is for a digestion using cDNAs 1051–1042 and 1274–1265. Shown in parentheses are the expected size of the fragment generated by the pair of oligoDNAs utilized and the size of the PHONTs (12 bases for PHONT 1892 and 10 for PHONT 1093). When cDNAs are utilized, the expected size represents the midpoint of the expected range ($\pm$ 10 nucleotides) of products, arising from possible RNase H cleavage along the length of the RNA:DNA heteroduplexes.

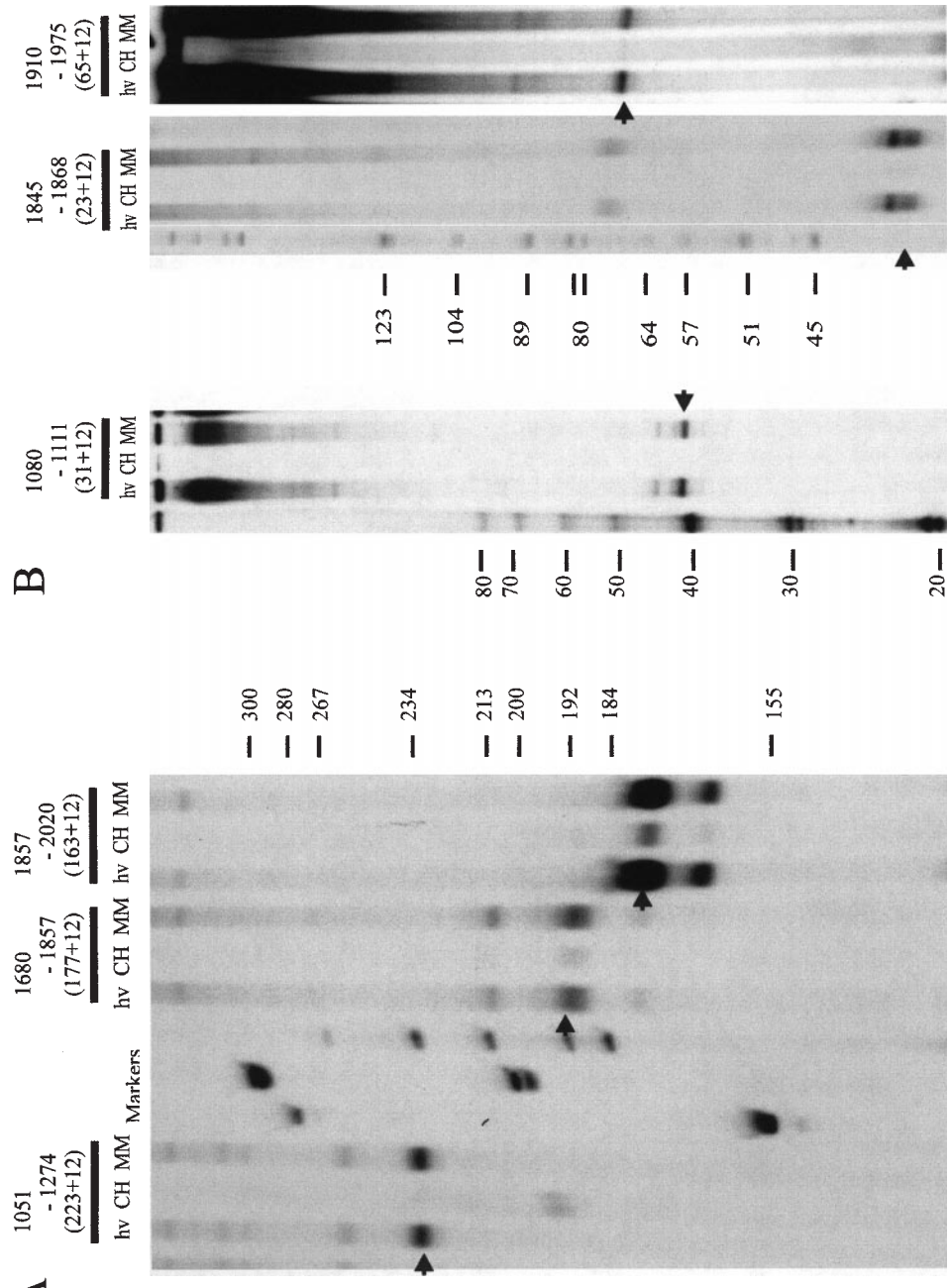
A
1051 - 1274 (223+12)
hv CH MM
Markers
1680 - 1857 (177+12)
hv CH MM
1857 - 2020 (163+12)
hv CH MM
300
280
267
234
213
200
192
184
155
B
1080 - 1111 (31+12)
hv CH MM
1845 - 1868 (23+12)
hv CH MM
1910 - 1975 (65+12)
hv CH MM
123
104
89
80
64
57
51
45
80
70
60
50
40
30
20

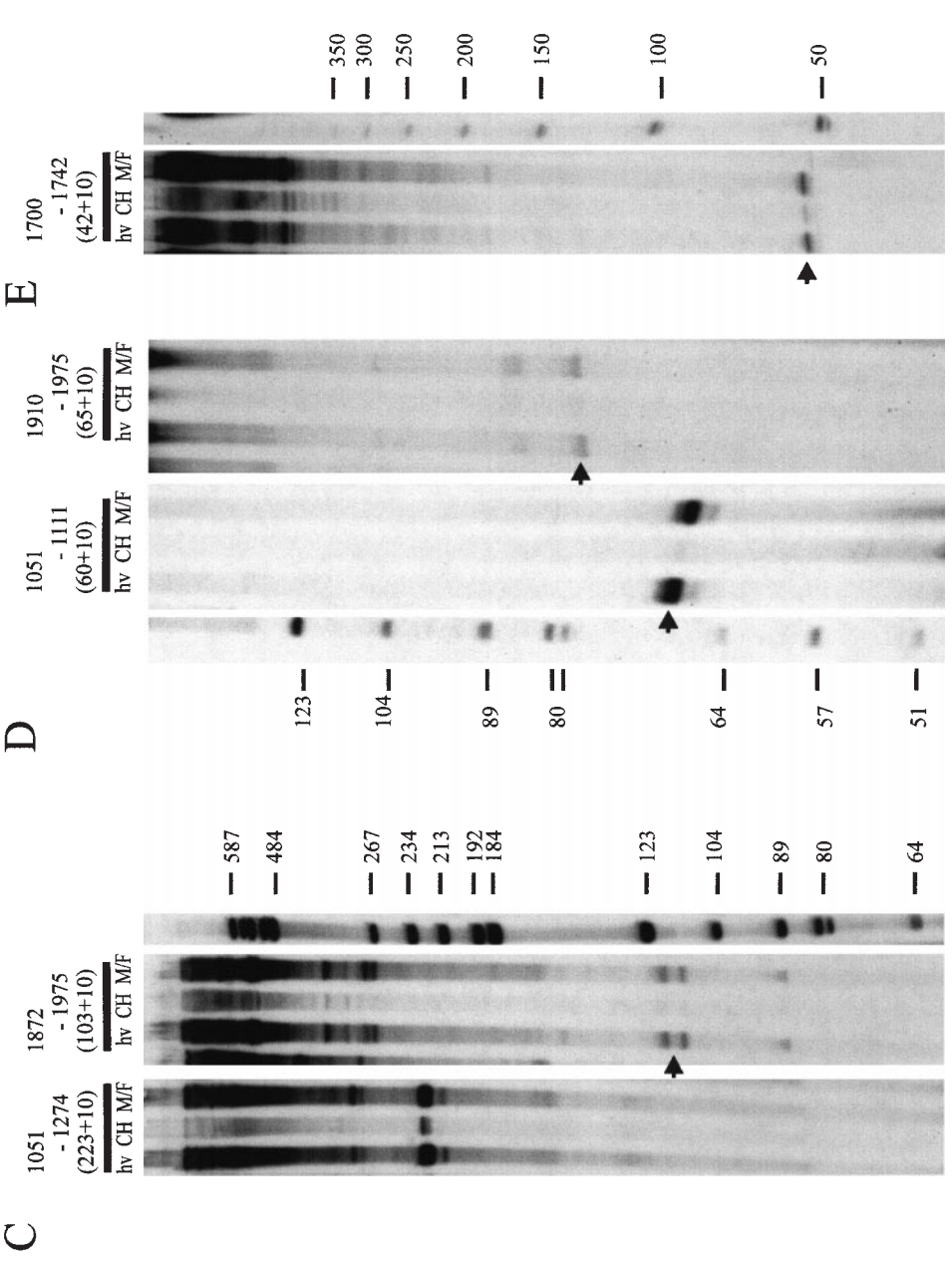

FIG. 3. *Continued.*

TABLE 3

Relative Yields of Target Site-Specifically Labeled RNase H Fragments

p*PHONT	Labeled fragment	Cleavage efficiency	Corrected relative yield of labeled fragment[a]
	1060–1111	0.92	0.39 ± 0.04
1892	1845–1910	0.40	(1.00)
	1910–1975	0.85	0.20 ± 0.04
	1051–1111	0.55	(1.00)
1093	1701–1764	0.71	0.18 ± 0.03
	1910–1975	0.85	0.38 ± 0.02

[a] Corrected for cleavage efficiency.

approximately stoichiometric levels with 50S subunits, it selectively inhibits p*PHONT 1892 photoincorporation into 23S rRNA fragment 1051–1111, presumably by direct steric interference, but does not affect photoincorporation into fragment 1845–2020 (Figs. 4A and 4B). On the other hand, in accord with its noncompetitive inhibition of p*CHASE 1093 binding (Fig. 2), added TS decreases p*PHONT 1093 photoincorporation into all three fragments, 1051–1111, 1700–1816 and 1910–1975 (Figs. 4C and 4D).

Photoincorporation of PHONTs 1892 and 1093 does not proceed via 50S dimer. The modest yields of photoincorporation of PHONTs 1892 and 1093 (Table 2), coupled with the surprising nature of the some of the crosslinks identified (see *Discussion*), raises the question as to whether photoincorporation proceeds via a putative dimeric form of 50S, present in small quantities, in which crosslinking occurs between subunits. Although we have been unable to find a published report of such a dimer, its possible presence in small quantities cannot be rigorously excluded. Two approaches were employed to investigate this question, each measuring the yields of p*PHONT 1892 photoincorporation into fragment 1080–1111 and of p*PHONT 1093 into fragments 1701–1764 and 1910–1975. In the first, yields were measured as a function of 50S concentration (0.1–2.5 μM) at constant p*PHONT concentration (0.1 μM), and equal quantities of ribosomes were extracted for RNaseH digestion and SDS–PAGE analysis. If labeling occurred only via dimer, and dimer were present in a rapid, unfavorable equilibrium with monomer, then raising the concentration of 50S subunits should result in a large increase in the yields. In fact, the yields per 50S subunit show only minor variation with 50S concentration in this range (Fig. 5A). In the second approach, yields obtained for different fractions (I, II, and III, Fig. 5B) from a sucrose density gradient preparation of 50S subunits were compared. If 50S dimer were present in small amounts but not equilibrating with monomer, then the percentage of such dimer should be higher for fractions further into the gradient and the yield of labeled fraction should follow suit. No such trend was observed. We conclude that target site-specific labeling of the RNase H fragments in question occurs within the 50S monomer.

Identification of nucleotides target site-specifically labeled by PHONT 1892 target site. Specific sites of photoincorporation within the labeled fragments 1060–1111, 1845–1868, and 1910–1975 were identified by reverse transcriptase primer extension on 23S rRNA extracted from 50S subunits that were photolabeled by PHONT 1892.

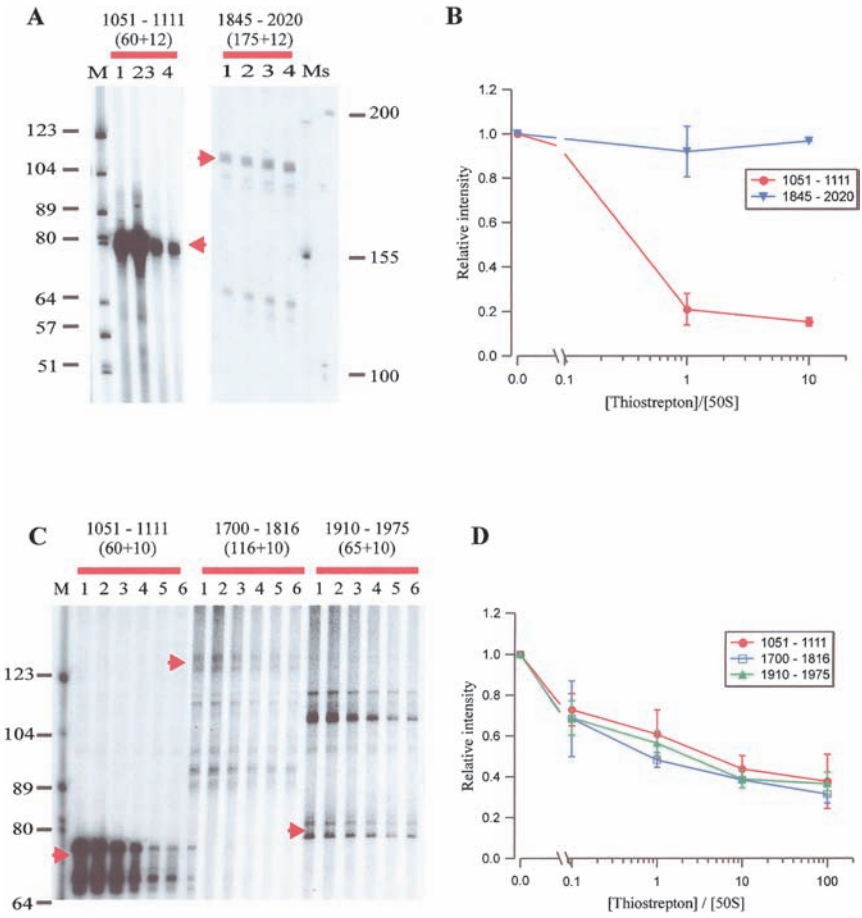

FIG. 4. Thiostrepton (TS) effects on the formation of PHONT-labeled RNase H fragments. Photolyses were carried out under standard conditions ([50S] = 1.5μM, [p*PHONT] = 0.5 μM) in binding buffer containing 1% DMSO unless otherwise specified. (A) Labeling by p*PHONT 1892. Lanes 1, no added DMSO; lanes 2, no TS; lanes 3, 1.5 μM TS; lanes 4, 15 μM TS; lanes M, size standards. (B) Plots of band intensity in part (A) vs. $[TS]_{total}/[50S]_{total}$. (C) Labeling by p*PHONT 1093. Lanes 1, no added DMSO; lanes 2, no TS; lanes 3, 0.15 μM TS; lanes 4, 1.5 μM TS; lanes 5, 15 μM TS, lanes 6, 150 μM TS lane M, size standards. (D) Plots of band intensity in part (C) vs. $[TS]_{total}/[50S]_{total}$. In (B) and (D), the band intensities were normalized against the intensity of the corresponding band in lane 2. Values shown are the average of data from 3–5 experiments.

These experiments were carried out at a PHONT 1892:50S ratio of 2:1 in order to maximize the stoichiometry of probe photoincorporation, thereby increasing the visibility of autoradiographic bands arising from primer extension stops or pauses (Fig. 6). Sites of photoincorporation were identified as the nts immediately following stop or pause sites (−1 in the 23S rRNA sequence). Three primers were employed to identify PHONT 1892 crosslinked sites. Primer extension using cDNA 1156–1140

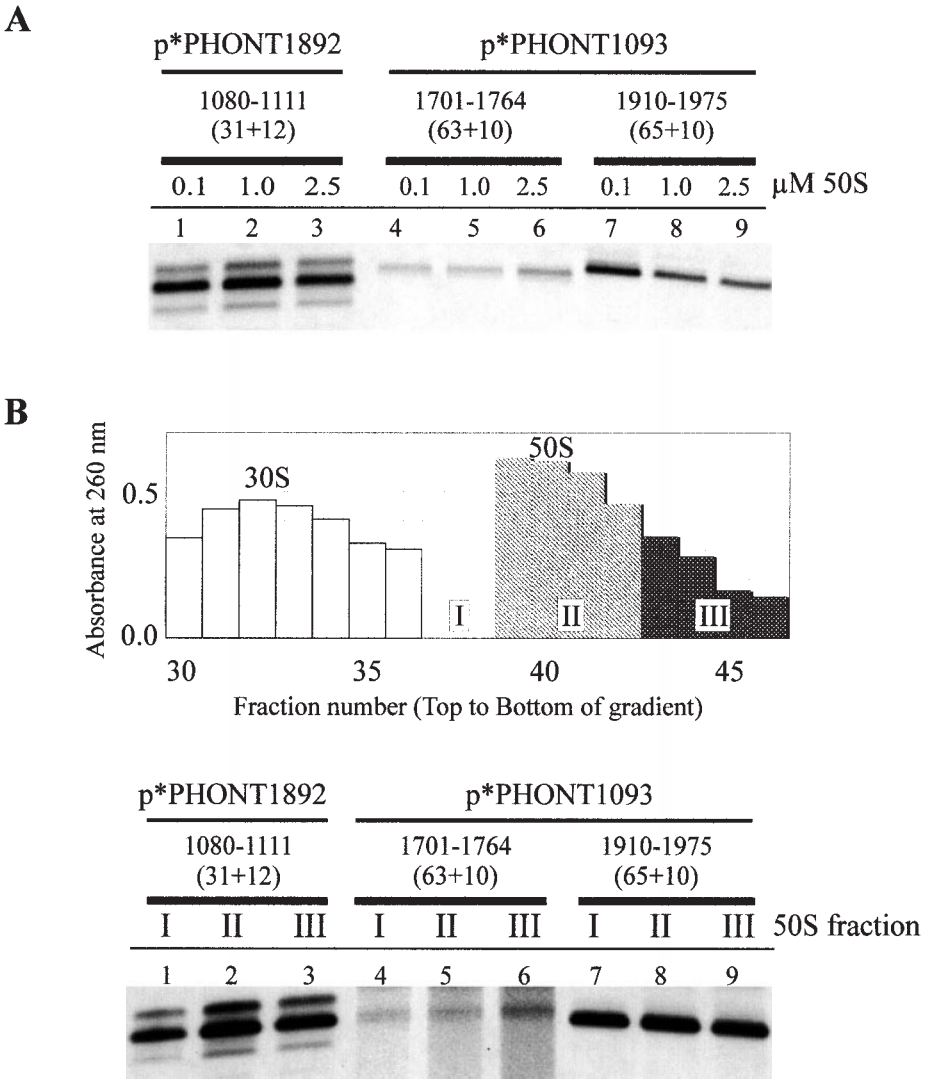

FIG. 5. Relative yields of p*PHONT-labeled RNase H fragments. (A) As a function of [50S]. Photolyses were carried out in the presence of 0.1 μM p*PHONT and the indicated [50S]. Apparent size of main band shown is given in parentheses. Lanes 1–3, p*PHONT 1892, fragment 1080–1111 (43 nts); Lanes 4–6, p*PHONT 1093, fragment 1701–1764 (73 nts); Lanes 7–9, p*PHONT 1093, fragment 1910–1975 (75 nts). (B) As a function of fraction in sucrose density gradient. 50S subunits used in photolyses were taken from different fractions (I, II, and III) of a 7.4–50% sucrose gradient, formed in a zonal rotor, as shown. Photolyses were carried out under standard conditions ([50S] = 1.5 μM, [p*PHONT] = 0.5 μM), using the indicated 50S fraction. Apparent size of main band shown is given in parentheses. Lanes 1–3, p*PHONT 1892, fragment 1080–1111 (43 nts); Lanes 4–6, p*PHONT 1093, fragment 1701–1764 (73 nts); Lanes 7–9, p*PHONT 1093, fragment 1910–1975 (75 nts).

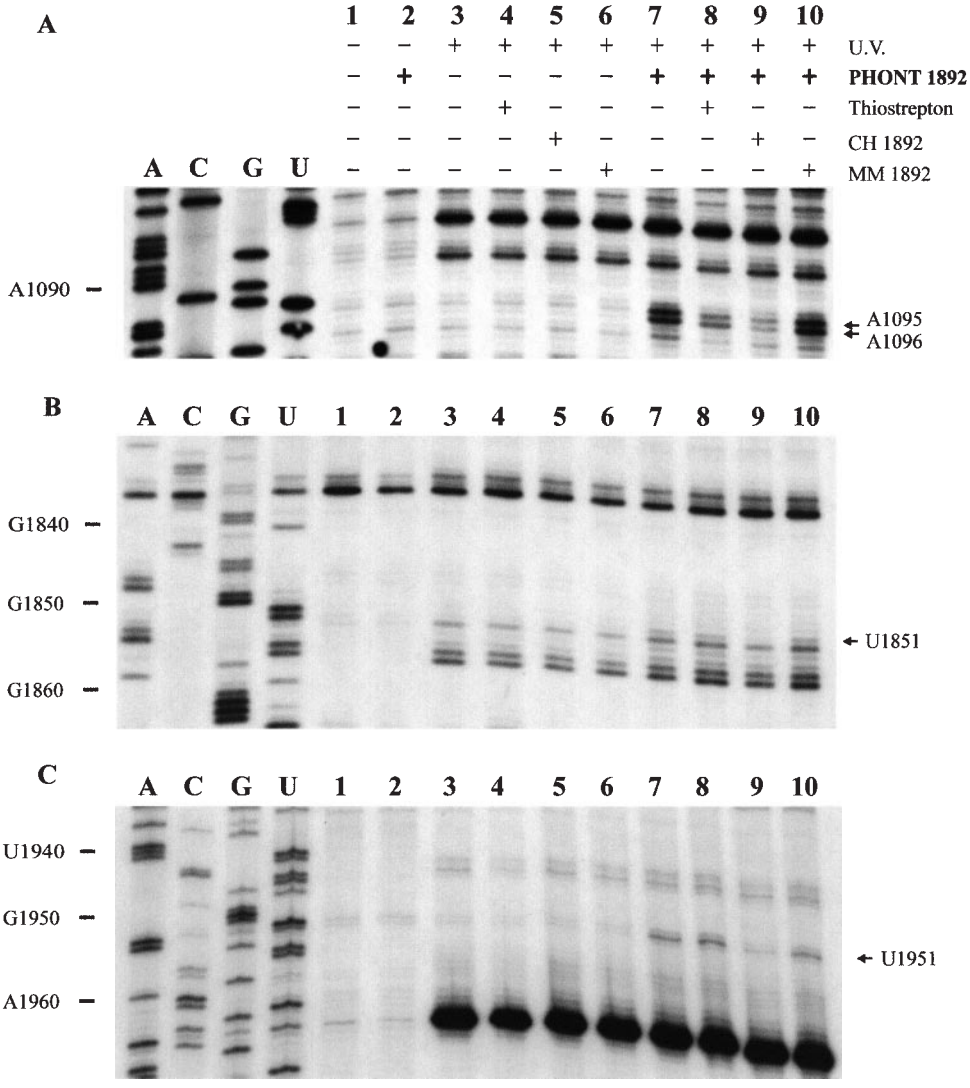

FIG. 6. Reverse transcription analyses of PHONT 1892-labeled 23S rRNA. Photolyses were carried out at as indicated with [50S] = 1.5 μM. When present, PHONT 1892 was added to a concentration of 3 μM, and CHASE 1892, MISMATCH 1892, and TS were each added to a concentration of 15 μM. Experiments containing TS were carried out in 1% DMSO. The cDNAs used as primers were: (A) 1156–1140; (B) 1922–1906; (C) 2042–2026. Lanes A, C, G, and U are sequencing products generated from control 23S rRNA in the presence of ddTTP, ddGTP, ddCTP, and ddATP, respectively. Arrows mark decreases in stop or pause intensity resulting from CHASE 1892 or TS addition.

identified U1094/A1095 as major sites of photoincorporation (Fig. 6A). Similar analysis with cDNA 1922–1096 and 2042–2026 permitted identification of G1850 (Fig. 6B) and G1950 (Fig. 6C), respectively, as photoincorporation sites. Each of these sites is labeled target site-specifically, as demonstrated by the effects of added CHASE

1892 and MISMATCH 1892. Consistent with the results presented in Fig. 4A, the intensity of the stops or pauses reflecting U1094/A1095 labeling decreased in the presence of thiostrepton, but stops reflecting G1850 and G1950 labeling were unaffected.

Identification of nucleotides site-specifically labeled from the PHONT 1093 target site. Identification of labeled nucleotides by direct reverse transcriptase primer extension on 23S rRNA was not possible in this case, in part because of the lower yield of photocrosslinking from PHONT 1093 than from PHONT 1892 (Table 1). Rather, we employed two approaches based on the recovery and utilization of the ^{32}P-labeled RNase H fragments. The first subjected the excised fragments to reverse transcriptase primer extension. Here the logic was to prepare a sample enriched in labeled fragment by exploiting the resolution afforded by SDS–PAGE in separating labeled and unlabeled fragments on the basis of their size difference. In such a sample, the pauses or stops due to crosslinking will be enhanced relative to what is seen for total 23S rRNA. In practice, primer extension was carried out on both labeled fragment, identified by autoradiography, and unlabeled fragment migrating slightly faster, as identified by methylene blue staining. For the results displayed in Fig. 7, the labeled fragments were 1051–1274, 1680–1845 and 1845–2002. Stops or pauses seen with the labeled fragments but not with the unlabeled fragments indicate sites of crosslinking. This approach led to identification of nts C1072, U1097, and U1101 (Fig. 7A), U1712, U1716, and C1748 (Fig. 7B), U1926 and U1931 (Fig. 7C) as crosslinked sites.

The last five of these crosslinks provide important evidence for conformational change in 50S subunits, and were examined by a second approach in which excised ^{32}P-labeled RNase H fragments 1701–1764 and 1910–1975 were subjected to RNase T1 digestion in the absence and presence of added oligo cDNAs, spanning the labeled RNAse H fragments (Fig. 8). Digestion of RNase H fragment 1701–1764 gives two labeled products, a major one migrating at 19 nt and a minor one migrating at 15 nt. As PHONT 1093 is 10 nts long, these products correspond to PHONT 1093-labeled RNase T1 fragments that are 9 and 5 nts long, respectively. The 1701–1764 sequence yields a unique 5 nt RNase T1 fragment, 1711-AUAUG-1715. There is no 9-nt RNase T1 fragment, but if one assumes that incorporation into U1716 would interfere with RNase T1 digestion at G1715, and then a strong candidate for the 9 nt fragment is 1711-AUAUGUAGG-1719, since digestion at a GG sequence is often difficult (*38*). This assignment is supported by the effects of added cDNAs (*39*). Formation of both the 15 and 19 nt fragments is strongly inhibited when RNase T1 digestions are carried out in the presence of cDNA 1718–1703, whereas addition of cDNAs 1735–1714 and 1752–1734 have lesser or negligible effects. These results strongly support the identification of U1712 and U1716 as crosslinked sites. On the other hand, the failure of RNase T1 digestion to generate a labeled fragment corresponding to 1745-AAAUCAG-1751 calls into question whether C1748 is a genuine crosslinked site. Furthermore, in contrast to added cDNA 1718–1703, added cDNA 1752–1734 does not affect the RNase T1 digestion pattern. However, both of these results may reflect false negatives, since covalently incorporated PHONT 1093 could interfere with RNase T1 digestion and with cDNA hybridization (see below).

RNase T1 digestion of ^{32}P-labeled RNase H fragment 1910–1975 generates one

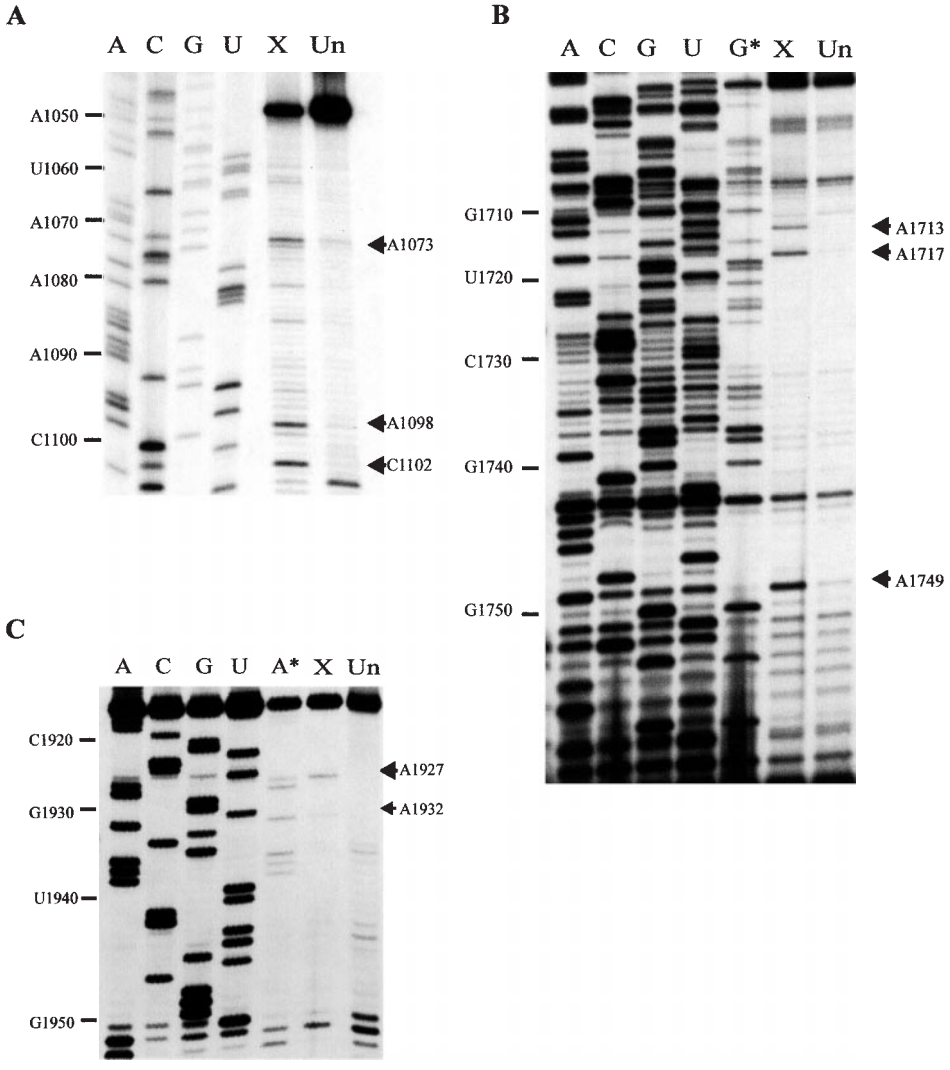

FIG. 7. Reverse transcription analyses of RNase H fragments derived from p*PHONT 1093-labeled 23S rRNA. Photolyses were carried out at [50S] = 1.0 μM and [p*PHONT 1892] = 1.0 μM. RNase H fragments of labeled 23S rRNA were generated and resolved as in Fig. 3, and gel slices containing p*PHONT-labeled fragments (lanes X) and unlabeled fragments (lanes Un) were eluted as described (see *Methods*), and used as templates for reverse transcription. (A) Fragment 1051–1274, primer cDNA 1156–1140; (B) Fragment 1680–1845, primer cDNA 1776–1750; (C) Fragment 1910–2011, primer cDNA 1983–1967. Lanes A, C, G, and U are sequencing lanes using 23S rRNA as template and lanes A* and G* are sequencing lanes using extracted unlabeled fragment as template.

major labeled product, which is 17 nt long, and corresponds uniquely to labeled 1923-UCCUAAG-1929. This result provides direct confirmatory evidence for crosslinking into residue U1926. Interestingly, added cDNA 1922/1934 did not inhibit formation

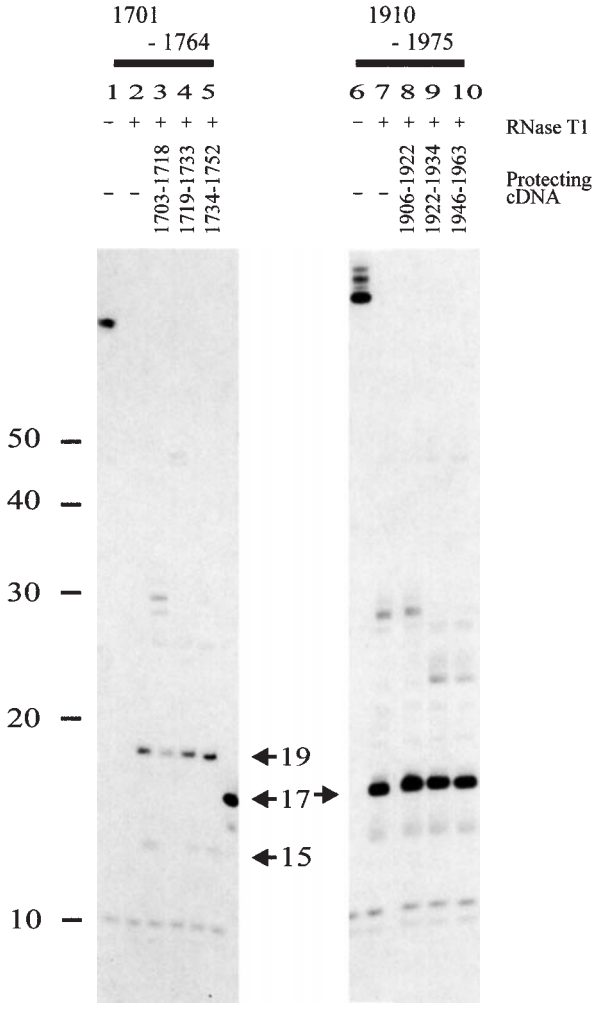

FIG. 8. RNase T1 digestion of RNase H fragments derived from p*PHONT 1093-labeled 23S rRNA. Labeled fragments, prepared as described in Fig. 7, were digested as described (see *Methods*) in the presence or absence of the indicated cDNAs. Fragment 1701–1764, lanes 1–5; Fragment 1910–1975, lanes 6–10. Arrows indicate sizes of RNase T1 fragments.

of this labeled product, illustrating the possibility of a false negative result using this approach.

Effect of CHASE oligonucleotides on chemical footprinting of 23S rRNA. To assess whether CHASE oligonucleotide binding caused structural distortion at regions neighboring photoincorporation sites, we examined whether addition of CHASE 1892 or CHASE 1093 in 10-fold excess (10 μM) over 50S subunits altered chemical footprinting (dimethyl sulfate and kethoxal) patterns in regions 990–1130 and 1700–1980 of 23S rRNA. No significant changes in chemical reactivity towards either modifying reagent was detected at sites other than the respective target sites (data not shown).

DISCUSSION

The results summarized in Table 4 identify four crosslinks, two each from PHONTs 1892 and 1093, that are incompatible with all three known 50S crystal structures (*10,12,15*), raising the question of whether such long-range crosslinks (denoted XLRs) are artifactual or are rather indicative of specific large scale motions within the 50S subunit. The crosslink formed between PHONT 1093 and U1926 (XLR 4), which may be considered as a quasi-reciprocal crosslink vis-à-vis XLR 1 (PHONT 1892 to U1094/A1095) since U1926 is only 28 ± 3 Å from C1892, argues in favor of the latter interpretation. Below we summarize the additional evidence that the observed XLRs are not artifacts, before considering their relationships to both conformational change and ribosome function.

XLRs are not artifacts. The most likely potential artifacts in XLR identification are: (a) misidentification of the sites of PHONT photoincorporation; (b) photoincorporation from a PHONT not bound to its targeted site; and (c) photoincorporation within a 50S subunit grossly perturbed by PHONT binding. Less likely are (d) that XLRs arise via crosslinking within a putative 50S dimer, from a PHONT bound in one monomer to a neighboring site within the second monomer and second, and (e) that apparent XLRs are due to large differences in the structure of *E. coli* 50S subunits vis-à-vis those from *T. thermophilus*, *H. marismortui*, or *D. radiodurans*.

We consider potential artifacts (a) and (b) first. Our strategy for identifying a crosslinking site is to first narrow down the potential site of crosslinking using progressively smaller RNase H fragments, and then to use RT analysis of the limited region of 23S rRNA so identified to locate incorporation sites with precision. As the RNase H cleavage sites generated by added cDNAs or chimeric oligonucleotides lead to fragments of predictable size, there is little possibility that the fragments are misidentified.

TABLE 4

Summary of Crosslinks and Distance Measurements

From	To	Distance[a] (Å)
C1892 (Helix 68)	U1094–XLR 1A	108/116/107
	A1095–XLR 1B	112/118/106
	G1850	18/18/19
	G1950–XLR 2	70/71/70
G1093 (Helix 44)	C1072	15/15/13
	U1097	14/14/12
	U1101	15/16/15
	U1712–XLR 3A	123/129/113
	C1716–XLR 3B	124/129/121
	(C1748)	109/115/107
	U1926–XLR 4	83/91/85
	(U1931)	80/87/79

[a] 1st distance: *T. thermophilus* 50S subunit within 70S ribosome (*12*); 2nd distance: *H. marismortui* isolated 50 subunit (*11*); 3rd distance: *D. radiodurans* isolated 50 subunit (*15*). All distances are phosphorus to phosphorus.

It is reasonable to expect that modification of rRNA accompanying PHONT incorporation would yield a pause or a stop on RT analysis. As in all cases the nucleotides reported as crosslinked represent the only stops or pauses seen (−1) in the regions of sequence corresponding to the labeled RNase H fragments, there is little basis for a misidentified crosslink. For PHONT 1892, this conclusion is further buttressed by the various controls shown in Fig. 6. Thus, XLRs 1A/B and 2 (Table 4) are only seen on irradiation of the PHONT 1892.50S complex. They are not seen in the absence of irradiation or of PHONT 1892, and they are blocked by addition of CHASE 1892, which should compete with PHONT 1892 for binding to the target site, but not by MISMATCH 1892, which should compete less well, if at all. These results provide strong evidence against potential artifact (b). Here it is important to note the closest fortuitous matches to nts 1882–1892 in 23 S rRNA had ≥3 mismatches, so binding of PHONT 1892 to such sites is extremely unlikely.

These controls at the RT analysis level could not readily be carried out for p*PHONT 1093. Rather, the approach used was to show that labeling of limited size RNase H fragments (1700–1742 and 1910–1975) containing XLRs was target site-specific (blocked by CHASE 1093, but not by MISMATCH 1093 or any of the FORMATCH 1093s) and then to use extracted ^{32}P-labeled RNase H fragments for RNase T1 and RT analyses. The former analyses clearly show target site-specifically labeled oligonucleotides 1711–1715, 1711–1719, and 1923–1929, consistent with the results of the latter analyses showing crosslinking into U1712 , U1716 (XLR 3A/B), and U1926 (XLR 4). The identifications of C1748 and U1931 as site-specifically labeled must be considered more tentative, since they are not confirmed by RNase T1 analysis, although each is close in the three-dimensional structure of 50S subunits to a confirmed labeled site (C1748 to U1712/1716, U1931 to U1926).

With respect to potential artifact (c), while conformational change at the immediate site of PHONT binding is expected, chemical footprinting shows no evidence for conformational change accompanying PHONT 1892 or PHONT 1093 binding in the regions containing long-range crosslinks. Similar results have been obtained in chemical footprinting studies of other complementary oligonucleotide binding to 30S or 50S ribosomal subunits (*4*). Furthermore, electron microscopy studies at a resolution of ~25 Å (*40,41*) show no evidence for conformational change following complementary oligonucleotide binding to 30S subunits. The relatively high affinities of PHONT 1892 and PHONT 1093 for 50S subunits (Fig. 2) also argues against large-scale conformational change induced by oligonucleotide binding since, as pointed out elsewhere (*3*), the energy required to induce such change would necessarily have to be taken from the intrinsic binding energy for PHONT binding.

As there are no published reports of 50S dimers, potential artifact (d) is quite hypothetical. Clearly, if 50S dimers exist, they are present in very small quantities. The experiments presented in Fig. 5, showing little or no dependence of crosslink yields on either 50S concentration or the sucrose gradient fraction of a 50S preparation, effectively rule out putative 50S dimers as the source of the observed XLRs. Last, concerning potential artifact (e), the crystal structures of 50S subunits from three different bacteria confirm the high degree of conservation of the bacterial 50S structure. While it is true that specific regions may show differences, especially where 23S rRNA 2° structure is not conserved, such differences are unlikely to account for XLRs

1A/B, 2 and 4, which involve nucleotides that are within highly conserved rRNA regions. In contrast, XLR 3A/B involves crosslinks to U1712 and U1716, which fall within a nonconserved portion of helix 63 stem-loop that is considerably longer in *E. coli* 23S rRNA (35 nts) than in *T. thermophilus* (29 nts), *H. marismortui* (23 nts), or *D. radiodurans* (19 nts). While this lack of conservation introduces some uncertainty into the 1093–1712/1716 distances shown (Table 4), the distances are so large that, despite this uncertainty, classification of the 1093–1712/1712 crosslinks as an XLR is secure.

Mechanism of XLR formation. If XLRs are not artifacts, how are they formed? From the published 50S structures it is clear that all of the nucleotides involved in XLRs 1–4 are found on the surface of the 50S particle, in regions that are relatively free of protein (Fig. 9A). We surmise that such regions could be inherently flexible, allowing large-scale movements leading to alternative 50S conformations that permit XLR formation. In this context four questions are of particular interest. What is the evidence that the pertinent regions are flexible? How much movement from the conformation(s) seen in the crystal structure is required for XLR formation? What evidence is there for the presence of alternative conformations giving rise to XLR formation? What else is known about ribosome structure that could account for XLR formation?

Of the nucleotides involved in XLRs 1–4 (Table 4), 1093–1095 and U1926 are clearly within flexible regions of the 50S subunit. Thus, Yusupov *et al.* (*12*) describe four 23S rRNA regions showing high disorder in the 50S crystal structure. Nucleotides 1093–1095 fall within one of these, the L11 RNA binding domain, comprising nts 1030–1124 and including helices 42–44. A second such region is the 1915 stem loop (H69—nts 1906–1924), which is immediately adjacent to U1926. Additional X-ray and electron microscopy evidence for the flexibility of these two regions has been summarized recently (*12,15,16*). As well, there is evidence from footprinting experiments for the hinge-like nature of helix 42 (*4*). In addition, C1892 and G1950 fall within an important structural feature of the 50S subunit known as the lateral arm, which includes helices 68, 70, and 71 (the only connection of the 1915 stem loop to the rest of 23S rRNA is via a single-stranded loop to the lateral arm, accounting, at least in part, for its flexibilty). Although there is no direct evidence for the flexibility of the lateral arm, its importance for function (see below) has prompted speculation that movement of tRNA during the translational cycle could be coupled to conformational rearrangement of the noncanonical H70 segment (*12*).

Although the distances between the nucleotides involved in XLRs vary from 70–129 Å in the known crystal structures (Table 4), there are three factors which could decrease the movement required for XLR formation. The first is that, in both PHONTs, the sulfur of the photolabile s^4U group is up to 20 Å from the nearest base (C1892 and G1093, respectively) in the 23S structure (Fig. 1). Allowing for some fraying at the terminus of the new heteroduplex that accompanies PHONT binding to its target site, it is reasonable to consider that nucleotides approaching within 25 Å of C1892 or G1093 as being crosslinkable by the corresponding PHONT. The second factor is that there may be structural differences between the *E. coli* 50S subunit and those 50S subunits whose structures have already been determined, especially in flexible regions of the structure. It is reasonable to assume that such changes will be of the

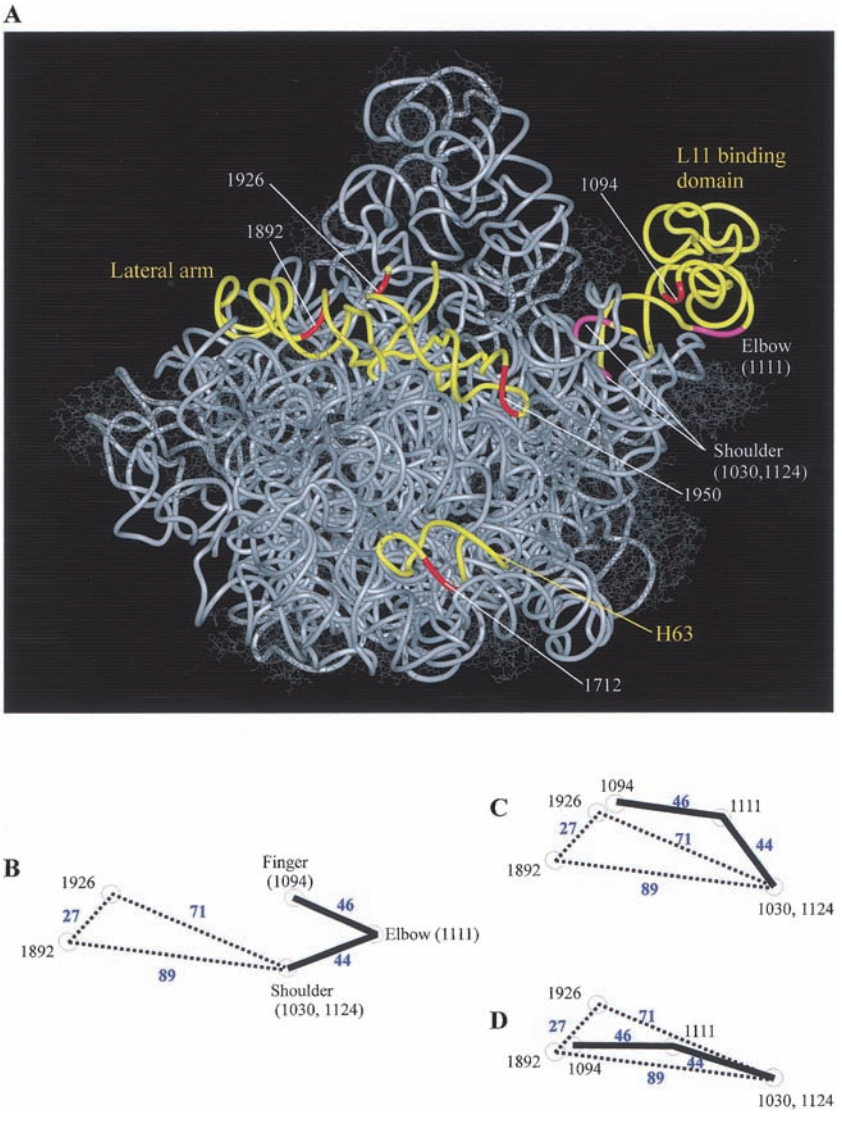

FIG. 9. The involvement of the L11 RNA binding domain in long-range crosslinks (XLRs). (A) 50S structure (*11*) indicating positions of nts U1094 (red), C1030 (purple), A1111 (purple), U1712 (red), C1892 (red), U1926 (red) and G1950 (red). Each of the specified nucleotides is in the middle of three continuous colored nucleotides. (B) Cartoon version of (A), emphasizing arm-like nature of L11 RNA binding domain. (C) Possible movement of L11 RNA binding domain arm, allowing formation of XLR 4. (D) Possible movement of L11 RNA binding domain arm, allowing formation of XLR 1.

same order of magnitude as the differences observed between the structures already determined (Table 4). Finally, formation of the new heteroduplex formed on PHONT binding will necessarily involve the breaking of some of the hydrogen bonds linking

the targeted sequence to the rest of the 50S subunit, allowing some displacement of this sequence from its original position. We estimate that the latter two factors might introduce an uncertainty of up to 25 Å in comparing XLRs to the known crystal structures. Adding all three factors together, lower limits of the relative movements required to form the four XLRs in Table 4 vary from 20–80 Å, although the actual movements could be somewhat larger.

Evidence that alternative conformations giving rise to XLR formation are present in solution comes from results presented in Table 3. Since photoincorporation into the target region will occur in all 50S conformations, the yields of photoincorporation into regions containing XLRs relative to the yields of photoincorporation into the target region provides some indication of the prevalence of conformations leading to XLR formation. For PHONT 1892, photoincorporation into fragments 1060–1111 (dominated by labeling of 1094/1095) and 1910–1975 (dominated by labeling of 1950) proceed at 39 and 20%, respectively, of the level seen in the target fragment (1845–1910). Similarly, for PHONT 1093, photoincorporation into fragments 1910–1975 (dominated by labeling of 1926, and, possibly, 1931) and 1701–1764 (dominated by labeling of 1712/1716 and, possibly, 1748) proceed at 38 and 18%, respectively, of the level seen in the target fragment (1051–1111). Because of the multiple factors that control photoincorporation yield, these percentages do not provide a direct measure of alternative conformations leading to XLR formation. Nevertheless, such conformations do not appear to be rare.

We envisage XLR formation as proceeding via Scheme 1, in which the dominant conformation, $50S_a$, is in equilibrium with an alternative conformation, $50S_b$, from which the XLR is formed, giving rise to the crosslinked subunit, $50S_x$. It is important to note that distances between the nucleotides involved in the crosslink may be greater in $50S_b$ than in $50S_x$; the free energy change accompanying bond formation could provide the necessary driving force for crosslinking sites in $50S_x$ that are too far apart for crosslink formation in $50S_b$.

$$50S_a \rightleftarrows 50S_b \rightarrow 50S_x$$

SCHEME 1

Nucleotides 1093–1095 fall within a particularly propitious region of the 50S subunit for XLR formation. In the 50S subunit crystal structure, the L11 domain extends as a bent arm from the body of the 50S subunit, with the upper arm corresponding to H42 having a length of 44 ± 2 Å (C1030 to A1111) and the lower arm, corresponding to H43 and H44, and their loops, having a length of 46 ± 1 Å (A1111 to A1094) (*11*,*12*,*15*). The positions of the shoulder (G1124, C1030), elbow (A1111), and finger (A1094) are positioned so as to form an approximately equilateral triangle, with the elbow extending furthest away from the body of the 50S subunit (Figs. 9A and 9B). Movement of this arm toward U1926 as shown in Fig. 9C, or, in a more extended form, toward C1892 (Fig. 9D), could be sufficient for formation of XLRs 1 and 4. Formation of XLR 1 (and of XLR 2) could also be aided by the local disruption in ribosome structure accompanying PHONT 1892 binding. Less dramatic movements of the L11 domain would be required if nucleotides U1926 and C1892

were also able to move toward nucleotides 1093–1095. Such movement of U1926 is quite likely, given the known plasticity of the 1915 stem loop region (*15*). Possible movement of C1892 is suggested by formation of XLR 2, which necessarily involves relative movement of C1892, in H68, toward G1950, in H71. Such movement could be accomplished by a bending of the lateral arm at the noncanonical helix, consistent with a previous proposal (*12*). Formation of XLR 3A/B (Table 4) requires the largest change from the known X-ray structures. Here even full extension of the L11 domain arm may be insufficient for crosslink formation, and it is likely that movement of the H63 stem-loop, which includes U1712 and U1716, is necessary. Such putative flexibility may be linked to the nonconserved length of the H63 stem-loop, as noted above.

Possible functional relevance of XLRs. Although other evidence for large-scale movement within the 50S subunit has been reported recently, particularly in the L1 and L11 regions (*15–17*), the XLRs characterized herein provide the first identification of specific nucleotides involved in such large-scale movements in solution. Even though the specific motions demonstrated in this study are unlikely to be directly relevant for an elongating 70S ribosome, because of steric clashes they would be expected to have with 30S subunit and with bound tRNAs and protein factors, they are nevertheless of interest in revealing the inherent flexibility of specific regions of 23S rRNA within the 50S subunit. It is possible that more limited motions of these regions are involved in the large conformational changes that the ribosome undergoes as it moves through its catalytic cycle (*12,15–18*). In this connection it is of interest that, with the exception of U1712 and U1716, the 23S rRNA nts involved in the XLRs have all been strongly linked to function. The L11 binding domain, including nts 1093–1095, binds thiostrepton [with a possible direct contact at A1095 (*26*)] and forms part of the binding site for EF-G, and movement of this domain has been implicated as an important part of the tRNA translocation process (*16*). The lateral arm, and its attached 1915 stem-loop region, includes nts C1892, U1926, and G1950, as well as four bridges to the 30S subunit. There is a direct interaction of C1892 with E-site bound tRNA position 71 that has been shown to be important for translocation (*42*) and the 1915 stem loop region contacts the D-stems of A- and P-tRNA, as well as the top of the penultimate stem (H44) of 16S rRNA, at the site of codon-anticodon interaction (*12*). In addition, the lateral arm interacts directly with the 2600 stem loop (H93) and the A loop (H92) of 23S rRNA (*12*), each of which is directly involved in the peptidyl transferase center (*20,43*).

In conclusion, our present results demonstrate the utility of the PHONT approach in identifying regions of intrinsic conformational lability in rRNA, some of which are known to be important for ribosomal function. The next step will be to use PHONT 1093 to probe 70S ribosomes, in both the absence and presence of tRNAs and factors (PHONT 1892 does not bind to 70S ribosomes because of the overlap of its target site with a bridge linkage to 30S subunits). Other regions of suspected conformational lability in both the 50S and 30S subunits are also amenable to the PHONT approach.

ACKNOWLEDGMENT

We gratefully acknowledge the excellent technical assistance of Ms. Nora Zuño in several technical aspects of this work.

REFERENCES

1. Singh, A., Thornton, E. R., and Westheimer, F. H. (1962) *J. Biol. Chem.* **237,** 3006–3008.
2. Chowdhry, V., and Westheimer, F. H. (1979) *Annu. Rev. Biochem.* **48,** 293–325.
3. Cooperman, B. S., Alexander, R. W., Bukhtiyarov, Y., Vladimirov, S. N., Druzina, Z., Wang, R., and Zuño, N. (2000) *Methods Enzymol.* **318,** 118–136.
4. Vladimirov, S. N., Druzina, Z., Wang, R., and Cooperman, B. S. (2000) *Biochemistry* **39,** 183–193.
5. Cooperman, B. S., Vladimirov, S. N., Bukhtiyarov, Y., Druzina, Z., Wang, R., and Seo, H.-S. (2000) in *The Ribosome: Structure , Function, Antibiotics and Cellular Interactions* (Garrett, R. A., Douthwaite, S. R., Liljas, A., Matheson, A. T., Moore, P. B., and Noller, H. F., Eds.), pp. 271–285, Am. Soc. Microbiol., Washington, DC.
6. Wang, R., Alexander, R. W., VanLoock, M., Vladimirov, S. N., Bukhtiyarov, Y., Harvey, S. C., and Cooperman, B. S. (1999) *J. Mol. Biol.* **286,** 521–540.
7. Mueller, F., and Brimacombe, R. (1997) *J. Mol. Biol.* **271,** 524–44.
8. Mueller, F., Sommer, I., Baranov, P., Matadeen, R., Stoldt, M., Wohnert, J., Gorlach, M., van Heel, M., and Brimacombe, R. (2000) *J. Mol. Biol.* **298,** 35–59.
9. Dolan, M. A., Babin, P. and Wollenzien, P. (2001) *J. Mol. Graph. Model.* **19,** 495–513.
10. Ban, N., Nissen, P., Hansen, J., Moore, P. B., and Steitz, T. A. (2000) *Science* **289,** 905–920.
11. Klein, D. J., Schmeing T. M., Moore, P. B., and Steitz, T. A. (2001) *EMBO J.* **20,** 4214–4221.
12. Yusupov, M. M., Yusupova, G. Z., Baucom, A., Lieberman, K., Earnest, T. N., Cate, J. H., and Noller, H. F. (2001) *Science* **292,** 883–896.
13. Wimberly, B. T., Brodersen, D. E., Clemons, W. M. Jr., Morgan-Warren, R. J., Carter, A. P., Vonrhein, C., Hartsch, T., and Ramakrishnan, V. (2000) *Nature* **407,** 327–339.
14. Schluenzen, F., Tocilj, A., Zarivach, R., Harms, J., Gluehmann, M., Janell, D., Bashan, A., Bartels, H., Agmon, I., Franceschi, F., and Yonath, A. (2000) *Cell* **102,** 615–623.
15. Harms, J., Schluenzen, F., Zarivach, R., Bashan, A., Gat, S., Agmon, I., Bartels, H., Franceschi, F. and Yonath, A. (2001) *Cell,* **107,** 679–688.
16. Agrawal, R. K., Linde, J., Sengupta, J., Nierhaus, K. H., and Frank, J. (2001) *J. Mol. Biol.* **311,** 777–787.
17. Frank, J. (2001) *Bioessays* **23,** 725–732.
18. Stark, H., Rodnina, M. V., Wieden, H. J., van Heel, M., and Wintermeyer, W. (2000) *Cell* **100,** 301–309.
19. Spahn, C. M., Beckmann, R., Eswar, N., Penczek, P. A., Sali, A., Blobel, G., and Frank, J. (2001) *Cell* **107,** 373–386.
20. Noller, H. F., Green, R., Heilek, G., Hoffarth, V., Hüttenhofer, A., Joseph, S., Lee, I., Lieberman, K., Mankin, A., Merryman, C., Powers, T., Puglisi, E. V., Samaha, R. R., and Weiser, B. (1995) *Biochem. Cell Biol.* **73,** 997–1009.
21. Brimacombe, R. (1995) *Eur. J. Biochem.* **230,** 365–383.
22. Cooperman, B. S., Wooten, T., Romero, D. P. and Traut, R. R. (1995) *Mol. Cell. Biol.* **74,** 1087–1094.
23. Uhlein, M., Weglohner, W., Urlaub, H., and Wittmann-Liebold, B. (1998) *Biochem. J.* **331,** 423–430.
24. Diedrich, G., Spahn, C., Schäfer, M. A., Wooten, T., Bochkariov, D. E., Cooperman, B. S., Traut, R. R. and Nierhaus, K. H. (2000) *EMBO J.* **19,** 5241–5250.
25. Moazed, D., Robertson, J. M., and Noller, H.F. (1988) *Nature* **334,** 362–364.
26. Rosendahl, G. and Douthwaite, S. (1994) *Nucleic Acids Res.* **22,** 357–363.
27. Wimberly, B. T., Guymon, R., McCutcheon, J. P., White, S. W., and Ramakrishnan, V. (1999) *Cell* **97,** 491–502.
28. Conn, G. L., Draper, D. E., Lattman, E. E., and Gittis, A. G. (1999) *Science* **284,** 1171–1174.
29. Buck, M. A., Olah, T. A., Weitzmann, C. J. and Cooperman, B. S. (1989) *Anal. Biochem.* **182,** 295–299.
30. Tracy, S. (1981) *Prep. Biochem.* **11,** 251–268.
31. Skripkin, E. A., Kopylov, A. M., Bogdanov, A. A., Vinogradov, S. V., and Berlin, Y. A. (1979) *Mol. Biol. Report* **5,** 221–224.
32. Hill, W. E., Weller, J., Gluick, T., Merryman, C., Marconi, R. T., Tassanakajohn, A., and Tapprich, W. E. (1990) in *The Ribosome: Structure, Function, and Evolution* (Hill, W. E., Dahlberg, A., Garrett, R. A., Moore, P. B., Schlessinger, D., and Warner, J. R., Eds.), pp. 253–261, Am. Soc. Microbiol., Washington, DC.
33. Almehdi, M., Yoo, Y. S., and Schaup, H. W. (1991) *Nucleic Acids Res.* **19,** 6895–6903.

34. Alexander, R. W., Muralikrishna, P. and Cooperman, B. S. (1994) *Biochemistry* **33,** 12109–12118.
35. Highland, J. H., Howard, G. A., Ochsner, E., Hasenbank, R., Gordon, J., and Stöffler, G. (1975) *J. Biol. Chem.* **250,** 1141–1145.
36. Thompson, J., and Cundliffe, E. (1991) *Biochimie* **73,** 1131–1135.
37. Xing, Y., and Draper, D.E. (1996) *Biochemistry* **35,** 1581–1588.
38. White, M. D., Rapoport, S., and Lapidot, Y. (1977) *Biochem Biophys Res. Commun.* **77,** 1084–1087.
39. Rosen, K. V., Alexander, R. W., Wower, J., and Zimmermann, R. A. (1993) *Biochemistry* **32,** 12802–12811.
40. Lasater, L. S., Montesano-Roditis, L., Cann, P., A., and Glitz, D. G. (1990) *Nucleic Acids Res.* **18,** 477–485.
41. Oakes, M. I., and Lake, J. A.. (1990) *J. Mol. Biol.* **211,** 897–906.
42. Feinberg, J. S. and Joseph, S. (2001) *Proc. Natl. Acad. Sci. USA* **98,** 11120–11125.
43. Kim, D. F. and Green, R. (1999) *Mol. Cell* **4,** 859–864.
44. Inoue, H., Hayase, Y., Iwai, S., and Ohtsuka, E. (1988) *Nucleic Acids Symp Ser.* **19,** 135–138.